Enzyme-Graphene Nanometal biohybrid Architectures as Highly Efficient Multifunctional Catalysts for Cascade Reactions

Noelia Losada-Garcia[a], Esteban P. Urriolabeitia[b] and Jose M. Palomo*[a]

[a] Department of Biocatalysis. Institute of Catalysis (CSIC). Marie Curie 2, 28049 Madrid, Spain.

E-mail: josempalomo@icp.csic.es

[b] Instituto de Síntesis Química y Catálisis Homogénea (ISQCH). CSIC-Universidad de Zaragoza

Pedro Cerbuna 12, 50009 Zaragoza, Spain

Abstract

The development of new catalytic systems with different chemo- and biocatalytic functionalities for sustainable one-pot multistep transformations represents a big challenge in modern chemistry. Here, we have designed and synthesized novel enzyme-graphene nanometal hybrids of palladium and copper as multiactive heterogeneous catalysts. The *in-situ* formation of metallic nanoparticles of different size and species on enzymes (*C. antartica lipase*, CALB and and *T. lanuginosus* lipase), TLL) immobilized on multilayer graphene-anchored enzymes (G@CALB and G@TLL preparations) at room temperature and aqueous media allowed to create different kind of enzyme-metal nanoarchitectures, containing up to two enzymes and metallic nanoparticles of two different metals in the same compartment. The metallic nanoparticles were synthesized exclusively induced by the enzyme, homogeneously distributed on the enzymatic structure used as scaffold. The cooperative and synergistic participation of different chemo and biocatalytic components in the reduction process and especially in different cascade reactions was demonstrated. Domino cascade in aqueous media (enzymatic hydrolysis, metal reduction, and metal oxidation) was successfully performed from the different hybrid systems. The synthesis of glycoderivatives, transforming selectively peracetylated glucal to novel disaccharides, using **G@CALB-$Cu_3(PO_4)_2$NP**s and **G@CALB-Cu(0)NPs** or α-peracetylated glucose to diacetyl-gluconic acid by **G@TLL@CRL-$Cu_3(PO_4)_2$NPs** was successfully performed. Finally, the successful application in the dynamic kinetic resolution of racemic arylamine (>99% conversion and ee) in organic solvent catalyzed by **G@CALB-Pd(0)NPs-$Cu_3(PO_4)_2$NP**s demonstrated the potential effect in synthetic chemistry, and the synergistic effect of catalysis between enzyme and metals. Furthermore, recycling studies demonstrated the high robustness of them.

Introduction

Catalytic cascade reactions are considered one of the most sustainable ways to produce complex structures from relatively simple starting materials.[1-8] These processes present advantages when compared to the typical single reaction, such as atom economy, step-saving, and therefore high yield and efficiency of the chemical process. Among the different catalytic methodologies to perform cascade reactions, systems that combines the wide reactivity of chemocatalysts and the unbeatable selectivity of biocatalysts have shown great application potential in chemical synthesis.[9-10] However, a proper design of enzyme-metal combination is challenging, because these two types of catalysts often deactivate mutually and the reaction conditions for one cannot be applied to the other.[11] The rational integration of different catalytic modules into single hybrid nanoarchitectures without compromising their reactivity and stability is still a defiance due to their differences in composition, structure, size, surface chemistry, and active-site reactivity.

In order to fulfill this problem different alternatives have been developed in the recent years. One has been the direct incorporation of metals or organometallic complexes into a protein structure combining genetic and chemical tools, creating new artificial active sites.[12-16] Another successful approach has been the co-immobilization of both chemo- and biocatalytic systems in a solid material.[17] This methodology introduced the advantage of heterogeneous system although the compatibility of carriers and enzymes, insufficient exposure of active sites, low reactivity of the heterogeneous phase under ambient conditions, and poor molecular transport still remain as major hurdles in their use in cascade reactions.[18] Nanostructured materials, especially active nanoparticles (NPs), and biomaterials, as remarkable heterogeneous catalysts for different organic reactions, have undergone to an explosive growth thanks to the development of more efficient synthetic methodologies.[19-21] Under a catalytic point of view, nanostructures present many

advantages especially their large surface-to-volume ratio compared to bulk materials. Consequently, as catalysts, nanoparticles can be directly used as such or supported as different nanostructures (nanorods, nanotubes, etc.)[22-23] on a wide set of surfaces or biomolecules.[24-25] In this way, successful applicability of the metal nanoparticles in domino and cascade synthesis have been described.[26-29]

Recently, a third approach focusing on the development of chemoenzymatic cascade processes has been the combination of metal nanoparticles and enzymes. A very fancy approach combining metal nanoparticles with enzymes in the same solid material has been described for chemoenzymatic cascade processes.[30-33] A recent technology developed by our group has allowed to synthesize nanobiohybrid systems at room temperature in aqueous media where stable, small-sized, monodispersed metallic nanoparticles are *in situ* synthesized induced by an enzyme scaffold.[34-39] In comparison with other methods where metal nanoparticles are directly support on the solid phase, in this strategy enzyme acts a key role in the *in situ* synthesis of the nanoparticles, controlling their growth (being able to produce nanoparticles with very small size) and morphology.[40] Moreover, the nanoparticles thus synthetized are homogeneously dispersed around protein structure avoiding aggregation problems where this biological matrix conferred an extreme high stability. Another advantage of the system is that an enzyme-metal nanoparticle heterogeneous catalysts is formed. This strategy has shown that metal nanoparticles thus generated display an outstanding behavior in different chemical reactions under more sustainable conditions than those previously described.[34] However, in some cases, the remaining enzymatic activity of these nanobiohybrids after synthesis was partial or totally reduced,[38] limiting their application in cascade processes. Therefore, it seems necessary to develop a new strategy of synthesis of enzyme-metal nanoparticle hybrids, keeping the original activity and stability of the enzyme after hybrid

formation. In this term, the site-specific and selective immobilization of enzymes on solid supports in an active and stable form could fulfill this drawback. A homogeneously supported enzyme molecules could allow to synthesize *in situ* nanoparticles in such a way that more metal surface and more active sites could be available for catalytic performance in comparison with previous hybrids. In particular, the immobilization of lipases on hydrophobic supports have demonstrated to fixing exclusively the active open conformation of the enzyme.[40] Among different hydrophobic materials, graphene, a two-dimensional carbon-based nanomaterial, has been recently proposed as excellent platform for enzyme immobilization due to its large specific surface area and high electronic conductivity, biocompatibility and chemical stability.[41-42] Graphene is a basic component of materials with highly promising applications in areas such as electronics, materials, biomedicine, etc.[43-48]

Herein, we report the design and synthesis, for the first time, of a new type of hybrids based on biocatalytic immobilized preparations (graphene-enzyme) as scaffold containing metal nanoparticles. In these preparations, the enzyme fixes the optimal conformation for preserving full activity and stability, inducing nanoparticle formation exclusively on the protein matrix and controlling at the same time the nanoparticle size and distribution. We have prepared different kind of combined systems, from two components (one enzyme and one metal) up to four-components system (two enzymes-two metals). These new heterogeneous systems showed high catalytic efficiency and successful application in enzymatic, metallic and novel sustainable cascade processes under a variety of experimental conditions demonstrating their versatility and advanced performance of these systems as catalytic platforms.

Results and discussion

Preparation and characterization of G@Enzyme-CuNPs hybrids.

Graphite flakes were initially used to obtain graphene with immobilized lipase (G@Enzyme).[49] This strategy ensures the presence of lipase by fixing the open conformation and homogeneously dispersed on the solid material. This is due to the site-oriented interactions between hydrophobic graphene surface with particularly hydrophobic pocket area in the open conformation of lipase constitute by surrounding active site and lid area (Fig. S1). Using lipase from *Candida antartica* B (CALB), more than 95% of enzyme offered (5 mg/g) was immobilized in 10 min and the yield was quantitative after 30 min (Fig. S2). The enzyme activity was fully preserved (even hyper-activated) in the G@CALB preparation. The strength of the interaction between CALB and graphene was evaluated after incubating the preparation at relatively hard conditions -high temperature, presence of high concentration of solvents and detergent- and, in all cases, CALB was stable and no support leaching was observed (data not shown).

The synthesis of G@CALB-CuNPs heterogeneous hybrids was performed as shown in Fig. 1a. Small ultrafine copper nanoparticles (CuNPs) were synthesized by a mild-aqueous methodology, using copper sulfate and where site-oriented supported CALB acted as template and binder. The preparation started by mixing G@CALB in a phosphate solution at pH 7 with the copper salt, followed by a reducing step with $NaBH_4$ producing the formation of the heterogeneous hybrid. The superficial carboxylic groups moieties of Asp and Glu in CALB could bind with Cu^{2+} ions (Fig. 1b).

The fact that enzyme is immobilized fixing the open conformation with the active site and lid area interacting with the solid support, could cause an enzyme-Cu(II) binding exclusively on that groups in the opposite side, avoiding the potential interaction with Asp or His groups involved in

the catalytic triad of the enzyme (Fig. 1b-c). This could be critical to preserve the enzymatic activity after hybrid formation.

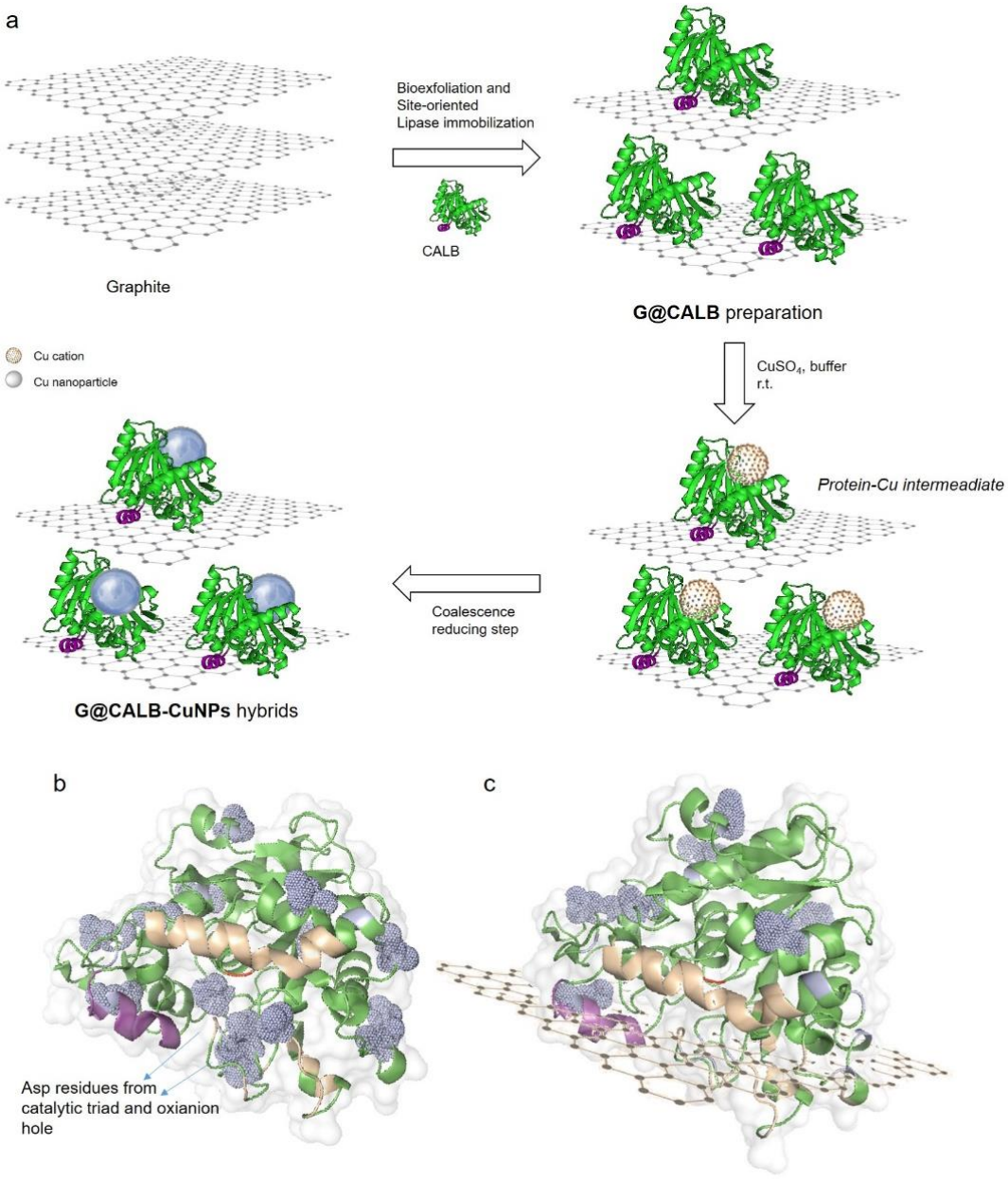

Fig. 1 Preparation and formation mechanism of G@CALB-CuNPs hybrids. (a) Synthetic scheme; (b) 3D-surface of CALB with several amino acid residues marked; (c) 3D-surface of CALB adsorbed on graphene layer with several amino acid residues marked. Asp and Glu residues (blue dots), hydrophobic groups (light brown), catalytic Ser (red), oligopeptide lid (purple). Figures were prepared using Pymol software and 1TCA PDB file from PDB data bank.

A full characterization of the hybrid was performed (Fig. 2 and S3-S5). Transmission electron microscopy (TEM) analysis revealed mainly the formation of small spherical nanoparticles with a diameter average size of 11 nm, as well as larger square nanoparticles (Fig. 2a-b and S3). The wide-angle X-ray diffraction (XRD) confirmed the presence of Cu_2O as mainly Cu species in this hybrid, by observation of four characteristic peaks, three of them assigned to planes (111), (200) and (220), respectively, of the fcc Cu lattice, with a minor fraction of Cu(0) (Fig. 2c and S3). Also, XRD pattern revealed that the immobilization of CALB and then the Cu_2O NPs formation did not change the crystal shape of the support (Fig. S1 and S3). X-ray photoelectron spectroscopy (XPS) was used to characterize the surface composition and electronic states of these Cu catalysts and the results confirmed the presence of Cu. The high resolution XPS spectrum of Cu 2p have peaks at 932.5 eV for Cu_2O and peaks at 934.39 eV and 955.00 eV for CuO (Fig. S4). FT-IR analysis also confirmed the presence of Cu_2O (Fig. S5). The inductively coupled plasma−optical emission spectroscopy results showed that the content of Cu in **G@CALB-Cu_2ONPs** was 7% (w/w).

A second approach for hybrid preparation was performed using sodium bicarbonate at pH 10 as buffer. The alkaline pH and the absence of phosphate on the media created a different copper species, which mainly was elemental Cu after reduction step. This higher pH could influence on the coordination of the Cu atom with the protein. While at pH 7 the coordination of Cu(II) is primarily by the carboxylic groups, at pH 10 other types of coordination may occur, for example with the alpha-amino group of the amino acids (pKa 9-11) or even with the NH_2 of the Lys residues (pKa around 10). XRD and XPS analysis confirmed the presence of Cu(0) (Fig. 2 and S6-7). XPS spectrum of Cu 2p after deconvolution showed a peak at 934.39 eV confirming the presence of traces of CuO on the surface (Fig. S7). FT-IR analysis also confirmed the presence of Cu (Fig. S8). The TEM analysis of **G@CALB-Cu(0)NPs** showed the formation of crystalline spherical

nanoparticles with an average diameter size of 8.3±0.5 nm nanoparticles (Fig. 2d-e and S4), slightly smaller than in the previous hybrid. ICP-OES determined the content of Cu of 4.74% in **G@CALB-Cu(0)NPs** hybrid.

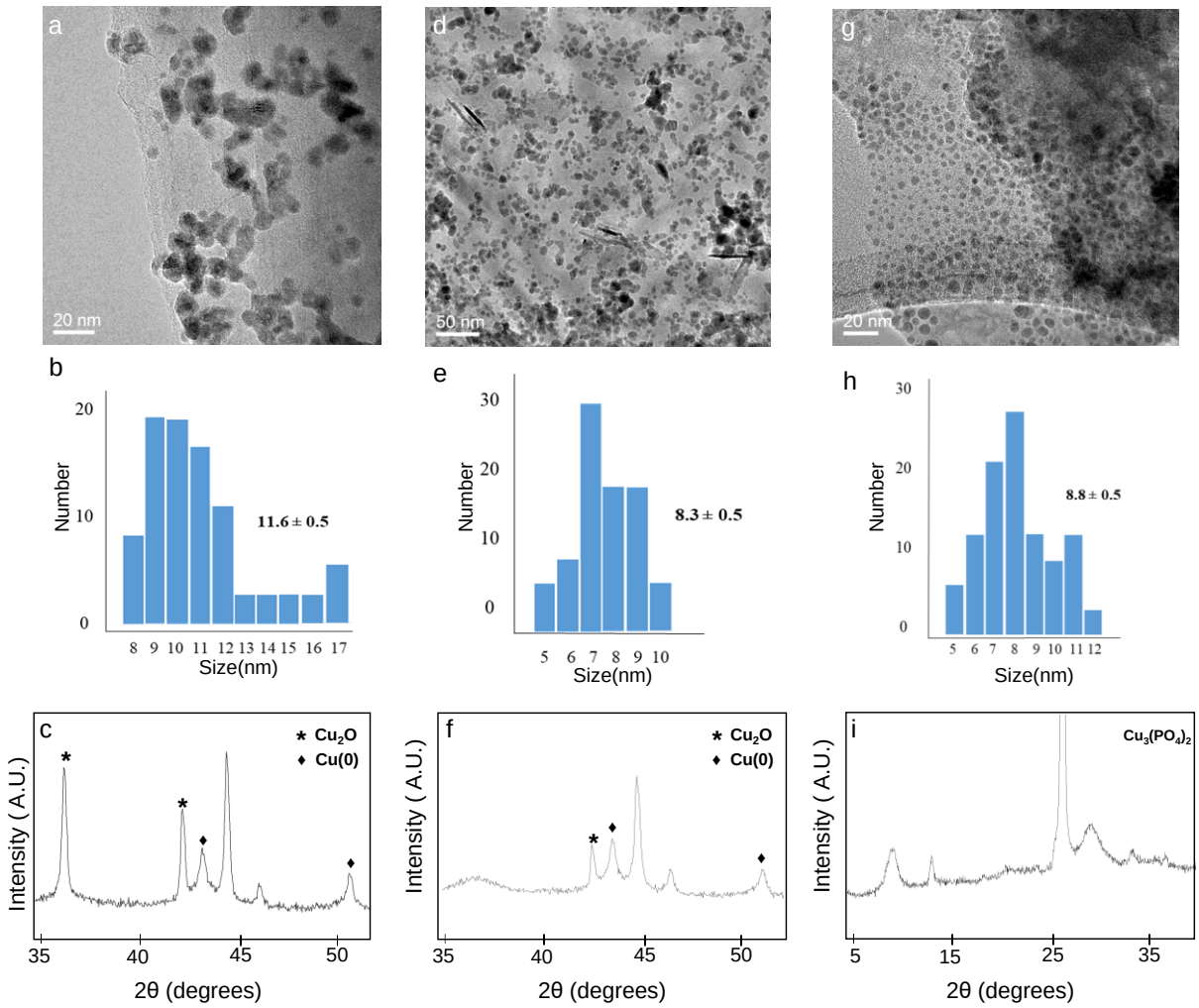

Fig. 2 (a) TEM image of **G@CALB-Cu_2ONPs;** (b) Particle-size distribution of Cu_2ONPs; (c) XDR pattern of **G@CALB-Cu_2ONPs**; (d) TEM image of **G@CALB-Cu(0)NPs;** (e) Particle-size distribution of Cu(0)NPs; (f) XDR pattern of **G@CALB-Cu(0)NPs**; (g) TEM image of **G@CALB-$Cu_3(PO_4)_2$NPs;** (h) Particle-size distribution of $Cu_3(PO_4)_2$NPs; (i) XDR pattern of **G@CALB-$Cu_3(PO_4)_2$NPs**.

A third approach was similar to the first, but avoiding the reducing step. TEM images showed the presence in this hybrid of spherical crystalline well-dispersed nanoparticles of an average diameter

size of 8.8±0.5 nm (Fig. 2g and S9). XRD and XPS analysis revealed $Cu_3(PO_4)_2$ as unique copper species (Fig. 2h and S9-10). Also, the structure was confirmed by FT-IR analysis (Fig. S11). The **G@CALB-$Cu_3(PO_4)_2$NPs** hybrid contained 6.53% of Cu determined by ICP-OES (Table S1).

In order to demonstrate that the copper nanoparticles were synthesized exclusively induced by the enzyme and only on the protein structure, G@CALB was chemically modified with polyethyleneimine (Mw800), blocking all accessible carboxylic groups in the protein (Fig. 1). Negligible amount of copper was detected in any of the three new hybrid synthesized using this treated graphene, confirmed by XRD (Fig. S12) and ICP-OES.

Next, the role of the protein structure in the formation of copper nanoparticles hybrids was studied. *Thermomyces lanuginosus* lipase (TLL), a typical lipase which mainly exists as dimeric form in solution in comparison with CALB which is monomeric,[50-51] was used. The more hydrophobic area around active site and a larger oligopeptide lid of this enzyme (Fig. S13) allowed to create an immobilized G@TLL with better graphene-exfoliation. Complete immobilization was achieved after 40 min incubation at room temperature (Fig. S13). The enzyme adsorbed on the graphene support showed even higher activity compared to soluble one (Fig. S13), due to fixing open monomeric conformation of the enzyme on the solid phase compared to the dimeric soluble form.[40] Therefore, following the procedures described previously, G@TLL-CuNPs heterogeneous hybrids were synthesized and fully characterized (Fig. 3a-c and S14-22), obtaining the so called **G@TLL-Cu_2ONPs, G@TLL-Cu(0)NPs** and **G@TLL-$Cu_3(PO_4)_2$NPs**. ICP-OES analysis determined that the content of Cu in all hybrids was similar, around 6% (Table S1). Surprisingly, TEM analysis revealed the formation of much larger copper nanoparticles in **G@TLL-Cu_2ONPs**, with two different average diameter sizes, 53 and 165 nm (Fig. 3a and S14). XRD analysis revealed Cu_2O as main species, containing a minor fraction of Cu (0) (Fig. S14). XPS analysis showed that apart

of Cu(I) also Cu(II) (CuO) exists in the surface of the nanoparticles (Fig. S15). A possible explanation of this large size of nanoparticles could be due to the reducing step. In this case, in G@TLL (where a graphene of 5-6 layers is formed), the reducing step is performed at pH 7, where energetic formation of hydrogen by sodium borohydride decomposition is generated. It is well described that this process could cause change in morphology and size of graphene[52] which seems to occur (Fig. 3a), affecting to the nanoparticle formation.

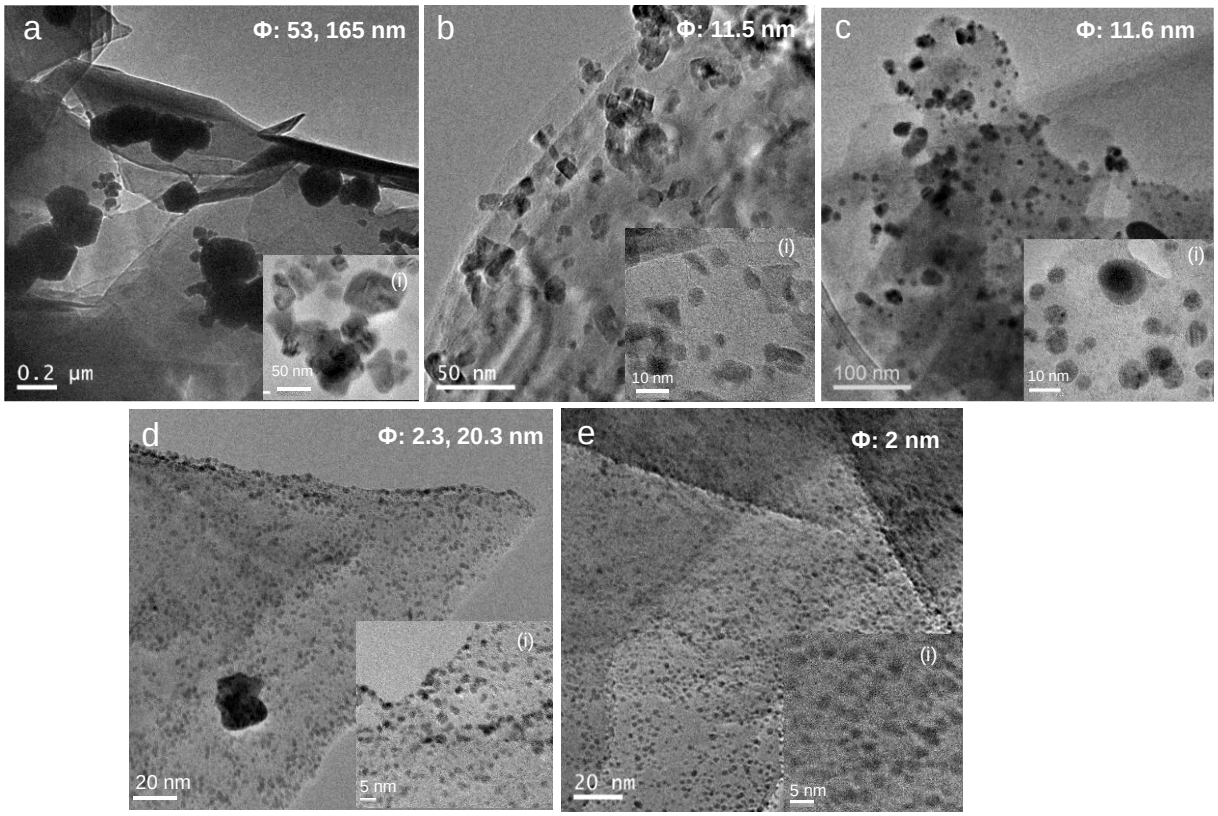

Fig. 3 (a) TEM image of **G@TLL-Cu_2ONPs;** (b) TEM image of **G@TLL-Cu(0)NPs;** (c) TEM image of **G@TLL-$Cu_3(PO_4)_2$NPs;** (d) TEM image of **G@CALB-Pd(0)NPs**; (e) TEM image of **G@TLL-Pd(0)NPs.** The insets show HRTEM images and average of particles size (i).

In the **G@TLL-Cu(0)NPs** hybrid, TEM analysis showed the presence of nanoparticles with different morphology (spherical, squares) with an average diameter size of approx. 11 nm (Fig.

3b), slightly larger compared to **G@CALB-Cu(0)NPs**. Although XRD analysis determined that main species was Cu (0), also Cu_2O was found (Fig. S17). This result can be attributed to the enzyme. XPS analysis also showed the presence of CuO in the nanoparticles surface (Fig. S18). The characterization of the **G@TLL-$Cu_3(PO_4)_2$NPs** hybrid showed the formation of spherical nanoparticles of approx. 11 nm average size of unique Cu^{2+} species (Fig. 3c and S20). These nanoparticles were slightly larger than those obtained in the previous hybrid using CALB. XRD, XPS and FT-IR analyses confirmed the presence of $Cu_3(PO_4)_2$ (Fig. S20-22).

In order to expand the applicability of this technology, Pd nanoparticles were synthesized at r.t. using G@CALB or G@TLL as template (Fig. 3d-e), adding palladium acetate in distilled water containing 20% (v/v) methanol. TEM analysis of **G@CALB-Pd(0)NPs** revealed the formation of very small size nanoparticles (2.5 nm average size) with a minor fraction with larger nanoparticles of around 20 nm (Fig. 3d), and XRD pattern revealed the formation exclusively of Pd(0) species (Fig. S23). XPS analysis, particularly of the core-line spectrum, confirmed the presence of elemental Pd by intense peaks at 338.46 eV, and traces of PdO with a small peak at 339.80 eV (Fig. S24). Elemental Pd was also confirmed by FT-IR (Fig. S25). ICP-OES experiment determined a Pd content of 1.6% (w/w). Similar results were obtained in **G@TLL-Pd(0)NPs,** where spherical nanoparticles with an average diameter size of 2 nm of Pd(0) species were determined (Fig. 3e and S26-28). This result showed the relevance of using G@TLL instead of soluble TLL, where the hybrid prepared using the latter contained also high percentage of PdO species (data not shown). [39] ICP-OES experiment determined a Pd content of 2.2% (w/w).

Preparation and characterization of G@TLL@CRL-MeNPs and G@Enzyme-Pd/CuNPs

Multifunctional systems combining two enzymes and/or metal nanoparticles catalysts were prepared as shown in Scheme 1. First, G@TLL@CRL-CuNPs hybrids were synthesized. *Candida rugosa* lipase (CRL) is a very important enzyme in selective biotransformations in carbohydrate chemistry,[53] however, the graphite bioexfoliation capacity of CRL was very low (10% immobilization), therefore the strategy was to produce a bienzymatic-graphene preparation by CRL immobilization on G@TLL (Scheme 1). When 20 mg CRL were offered to one gram of G@TLL, 50% immobilization was obtained (Fig. S29).

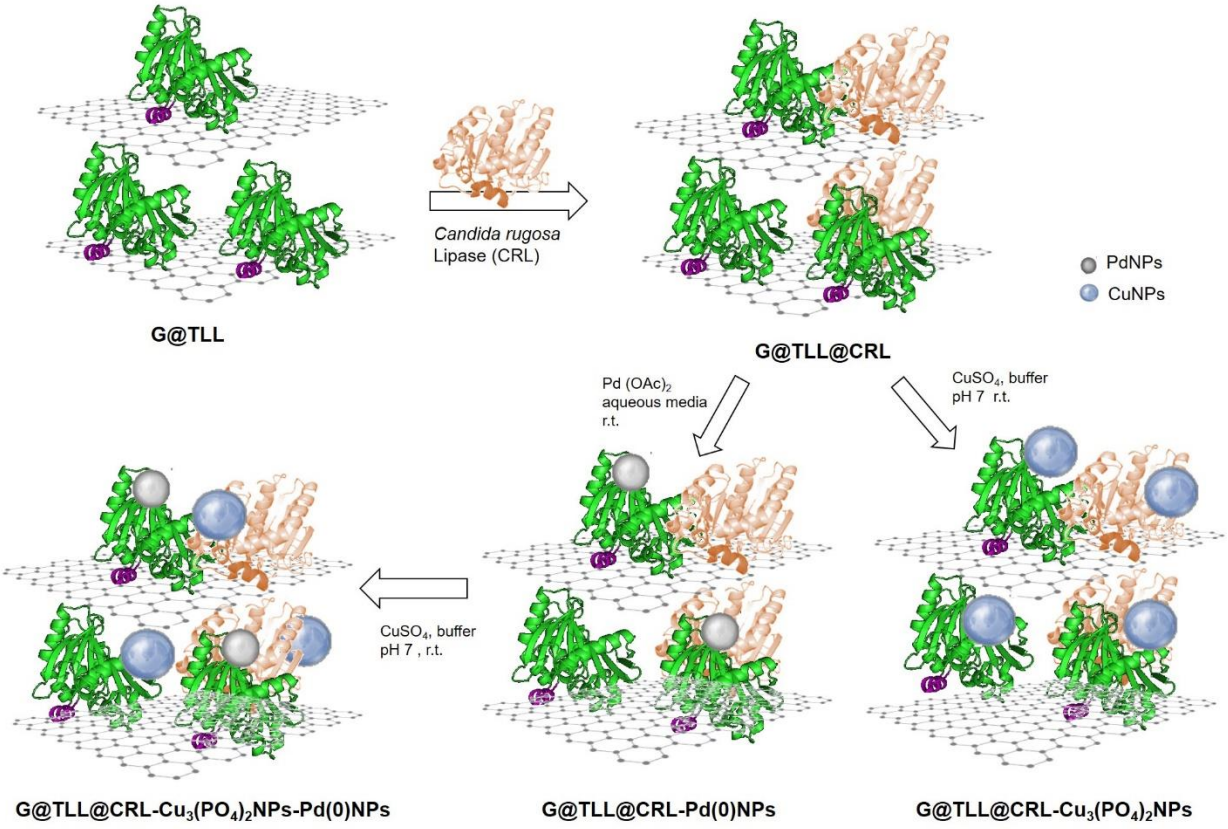

Scheme 1. Preparation of different G@TLL@CRL-MeNPs hybrids.

G@TLL@CRL was combined with copper salt following experimental conditions described in previous strategies to synthesize **G@TLL@CRL-Cu_2ONPs** and **G@TLL@CRL-$Cu_3(PO_4)_2$NPs** (Scheme 1, Fig. 4a-b and S30-31). The size and shape of formed nanoparticles in both cases varied from that using G@TLL. For example, in **G@TLL@CRL-Cu_2ONPs,** TEM analysis revealed the formation of nanoparticles in a more aggregated way because of both lipases, although much smaller than observed in **G@TLL-Cu_2ONPs** (Fig. 4a and S30). This could be due to a better stability of the graphene layers (Fig. 4a) in the reducing step with borohydride at pH 7 by the presence of both proteins. In the **G@TLL@CRL-$Cu_3(PO_4)_2$NPs** hybrid, TEM image showed formation of spherical nanoparticles with similar size than in **G@TLL-$Cu_3(PO_4)_2$NPs** (Fig. 4b and S31).

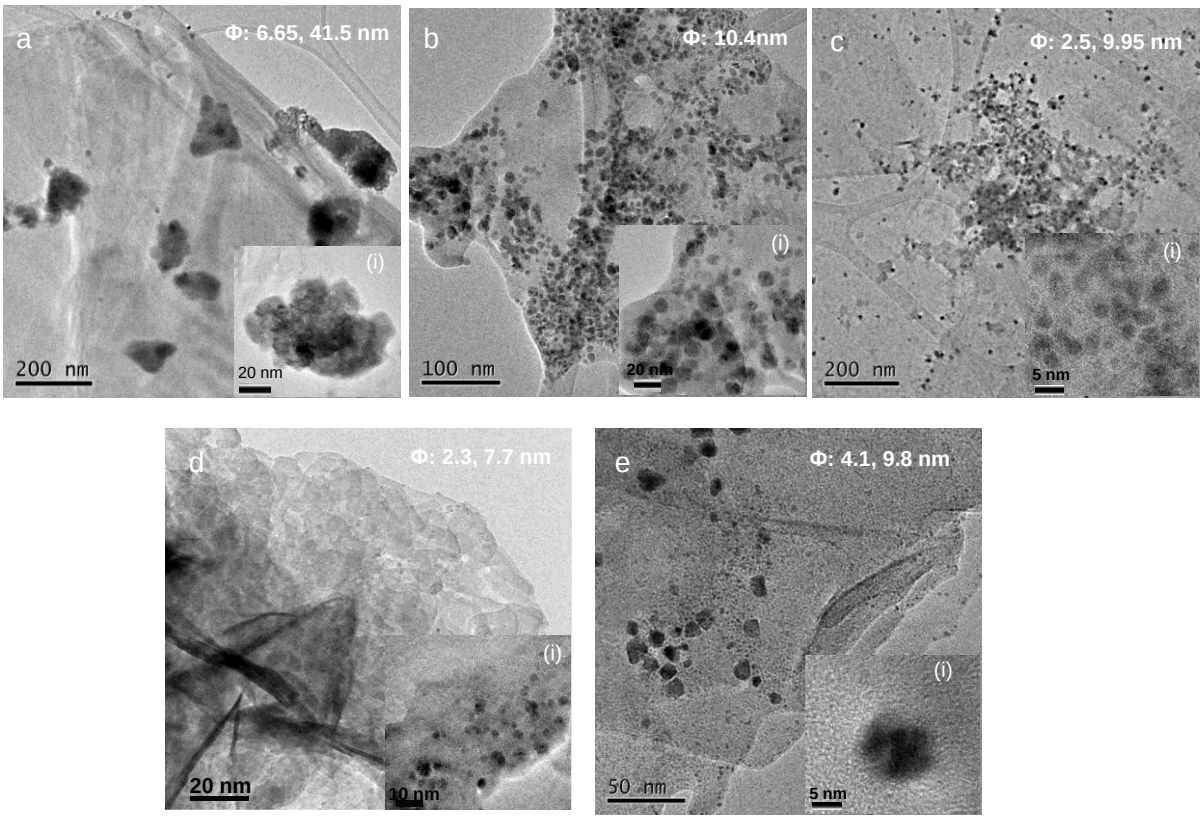

Fig. 4 (a) TEM image of **G@TLL@CRL-Cu_2ONPs;** (b) TEM image of **G@TLL@CRL-$Cu_3(PO_4)_2$NPs;** (c) **G@TLL@CRL-Pd(0)NPs**; (d) **G@CALB-Pd(0)NPs-$Cu_3(PO_4)_2$NPs;** (e) TEM image of **G@TLL@CRL-Pd(0)NPs-$Cu_3(PO_4)_2$NPs**. The insets show HRTEM images and average of particles size (i).

ICP-OES revealed that amount of copper in both cases increased when two lipases were on the support, 9.33% and 8.1%, respectively (Tables S1). In both cases, the presence of a second enzyme close to TLL makes the particles less dispersed, but also makes possible the control of the growth of the nanoparticles, reducing their size.

The bienzymatic preparation was also used as solid-phase template to prepare a PdNPs hybrid (**G@TLL@CRL-Pd(0)NPs**). The presence of CRL affected on the nanoparticles growth, and Pd(0) nanoparticles with two different sizes were obtained, the ones of 2.5±0.2 nm size, and other larger particles (9.95±0.5 nm) (Fig. 4c and S32). This result could be explained assuming that in the case of Pd, the coordination of metal ions to larger proteins resulted in larger nanoparticles.[27] ICP-OES analysis showed that the palladium content was only slightly higher, 2.77%.

Due to preceding results, we aimed to fabricate a three-component system (one enzyme-two metals) starting from **G@CALB** and a four-component system (two enzymes-two metals) starting from **G@TLL@CRL**. The **G@CALB-Pd(0)NPs-$Cu_3(PO_4)_2$NPs** and **G@TLL@CRL-Pd(0)NPs-$Cu_3(PO_4)_2$NPs** hybrids were synthesized by following the previous procedure. The first step of the synthesis involved the fabrication of the PdNPs hybrid, followed by the addition of copper sulfate in phosphate buffer at pH 7, as shown in Scheme 1.

In the characterization of **G@CALB-Pd(0)NPs-$Cu_3(PO_4)_2$NPs,** XRD analysis showed the presence of $Cu_3(PO_4)_2$ and elemental Pd as metal species (Fig. S33). TEM and STEM analysis revealed the formation of well-dispersed spherical crystalline PdNPs with an average diameter of 2.3±0.2 nm (similar size than in the G@CALB-PdNPs), although with a minor fraction with larger particles (7.7±0.5 nm) (Fig. 4d and S33). Surprisingly, TEM and STEM analyses revealed for copper, the formation of nanowires structures mainly (Fig. S33). A more precise STEM evaluation of the metal nanoparticles, by STEM high-angle annular dark field (HAADF) and corresponding

energy-dispersive X-ray spectroscopy (EDX) elemental mapping analysis, was made (Fig. S34). These analyses demonstrated the formation of a bimetallic $Cu_3(PO_4)_2$-Pd alloy nanoparticles. The surface Pd atoms were leached (demonstrated by ICP mass analysis) in the Cu nanoparticles formation from the metallic Pd. XPS analyses demonstrated the formation of more amount of PdO in the surface compared with the previous **G@CALB-Pd(0)NPs** (Fig. S35). The Pd vacancies in the shell were then crammed with $Cu_3(PO_4)_2$ core atoms to minimize the surface free energy of the catalyst. XPS and FT-IR analyses also confirmed the presence of these metal species (Fig. S35-36). The content of each metal in the hybrid was 1 % and 10% of Pd and Cu respectively, determined by ICP-OES.

For **G@TLL@CRL-Pd(0)NPs-$Cu_3(PO_4)_2$NPs**, TEM characterization revealed the formation of crystalline nanoparticles with two different average diameter sizes, 4.1±0.3 nm and 9.8±0.5 nm nm (Fig. 4e and S37). XRD, XPS and FT-IR analyses demonstrated the formation of $Cu_3(PO_4)_2$ as unique Cu species and Pd (0) as mainly Pd species (Fig. S37-39). XPS analysis of the core-line spectrum, confirmed the presence of elemental Pd by intense peaks at 338.46 eV, and also PdO with a small peak at 339.80 eV (Fig. S38). In this case the amount of PdO on the surface of the nanoparticles was higher than in the hybrid **G@TLL@CRL-Pd(0)NPs.** ICP-OES determined the content of Pd was 1.56% and 16% for Cu.

Enzymatic activity and stability of the different heterogeneous catalytic systems.

The enzymatic activity of these novel hybrids systems was evaluated using the hydrolysis of p-nitrophenyl propionate (**1**) as model reaction. Regular hybrid synthesized by this technology using lipases in soluble form showed almost negligible enzymatic activity after synthesis.[38] Therefore, it was not possible to apply them in chemoenzymatic cascade reactions. However, the new strategy to prepare the enzyme-metal nanoparticle hybrids in graphene allowed the enzymatic activity to

be preserved in all cases (Fig. 5), even when two metal nanoparticles were synthesized, where more than 25% of the initial activity was retained in the heterogeneous system.

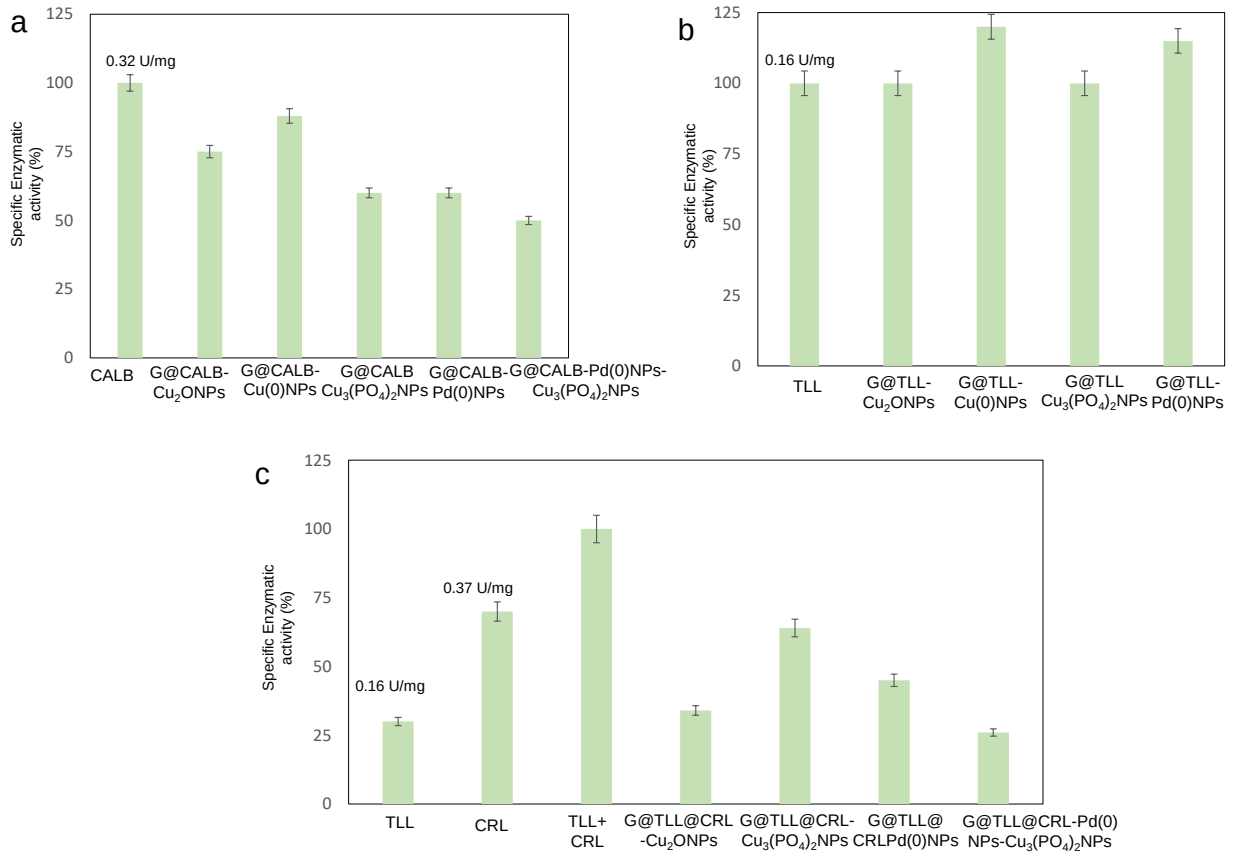

Fig. 5 Specific enzymatic activity of the different hybrids. (a) G@CALB hybrids; (b) G@TLL hybrids; (c) G@TLL-CRL hybrids.

The final enzymatic activity maintained in the different hybrids depended on the enzyme used as scaffold, the morphology of the nanoparticles and even the nature of the metal itself. Although the enzyme is fixed in open conformation with the active site exposed to the media, the potential presence of the nanoparticles located in the channel to the active site could affect the final enzymatic activity. This is especially relevant in CALB, taking into account that important COOH groups are located around this site.[51] **G@CALB-Cu(0)NPs** hybrid, which presents the smaller

nanoparticles formed (Fig. 2), conserved 85% of the initial activity for CALB (Fig. 5a). Also, the possible different coordination of the metal in this case could affect to the location on the protein structure. **G@CALB-Cu_2ONPs** and **G@CALB-$Cu_3(PO_4)_2$NPs** present larger nanoparticles and they showed lower enzymatic activity, although maintaining more than 60% in all cases (Fig. 5a). In the case of TLL, the oxyanion hole and the area surrounding active site are larger than in CALB[30c] and, although nanoparticles of Cu(0) are slight larger in **G@TLL-Cu(0)NPs**, the initial hyperactivation of the enzyme after graphene adsorption allowed to conserve even more than 100 % initial activity of TLL in solution. (Fig. 5b). As well, other Cu-hybrids conserved 100% initial activity. This could indicate that nanoparticle formation could also be in a different area, interfering less in the way of the substrates to the enzyme active site (high number of carboxylate residues in the surface, opposite to the active site[51]). In the hybrids with bienzymatic system (G@TLL@CRL), the final enzymatic remaining activity was affected by the synthetic methodology, with 70% activity remaining in **G@TLL@CRL-$Cu_3(PO_4)_2$NPs** (Fig. 5c). In the case of Pd, activity was slightly lower although nanoparticles size was smaller, maybe influence by the strategy used considering the use of co-solvent in the synthesis (Fig. 5).

A second coordination of nanoparticles in **G@CALB-Pd(0)NPs-$Cu_3(PO_4)_2$NPs** did not affected to the enzymatic activity (Fig. 5a), conserving 50% of initial activity. In **G@TLL@CRL-Pd(0)NPs-$Cu_3(PO_4)_2$NPs**, the enzymatic activity was slight decrease after Cu nanoparticles formation (Fig. 5c), maybe because of the highest amount of copper respect to the bimetallic hybrid using CALB, which could influence the substrate accessibility to the active site.

Finally, the stability of the different hybrids at different temperatures, or in the presence of different additives was evaluated (Fig. S40-S42) and no desorption of enzyme-metal system was observed in any case.

Application of biohybrid systems in domino cascade reaction

In order to evaluate the potential application of these heterogeneous biohybrids as multifunctional catalysts in single compartment, first they were tested in the cascade one-pot transformation of *p*-nitropropionate (**1)** to *p*-nitrophenol (**3**) in distilled water at room temperature as model reaction (Fig. 6a). All the different hybrid systems synthesized successfully performed the domino cascade reaction (Fig. 6b), demonstrating the dual-functionality of the hybrids with different combinations of enzymes and metal nanoparticles. It was demonstrated that the corresponding graphene-enzyme (G@CALB, G@TLL, G@TLL@CRL) preparations did not able to perform the cascade (Fig. 6b). Hybrids systems containing Cu(0)NPs or Pd(0)NPs completed the cascade conversion of **1** to **3** in 20-30 minutes (Fig. 6b). The highest overall activity of the **G@CALB-Cu(0)NPs** compared to other species seems to be due to several factors, such as enzymatic activity (first step) but mainly by the metallic one, based on the morphology of the nanoparticle (smaller size is related to the efficiency) and the metal valence (Cu(0)). For example, **G@CALB-Cu(0)NPs** showed a 1.38 fold times better enzymatic activity than **G@CALB-$Cu_3(PO_4)_2$NPs**, while this factor increases to 2-fold times faster catalysis considering the whole process (Fig. 6b). Moreover, **G@CALB-Cu(0)NPs** in a separate experiment needed 30 min to complete the hydrolysis of **1** to **2** however, it required 5 min to reduce **2** to **3** completely. The hybrid completed the domino cascade in 30 min, being 15% more efficient than separately, demonstrating the cooperative effect of the two activities in the same compartment. Also, similar results were observed in **G@TLL-Cu(0)NPs** which exhibited the highest efficiency in the cascade completing it in 20 min (Fig. 6b), which in comparison with other Cu hybrids exhibited 1.2 fold better enzymatic activity and faster metallic reaction. **G@CALB-Pd(0)NPs** needed 60 min for completing the cascade, whereas **G@TLL-Pd(0)NPs** need 30min (Fig. 6b).

a

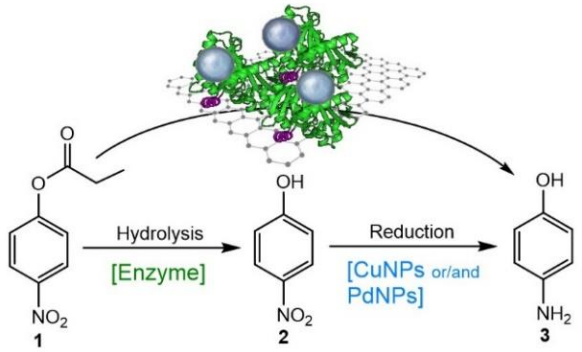

b

Catalyst	Time (min)	Conversion (%)	Yield (3) (%)
G@CALB	120	0	0
G@CALB-Cu_2ONPs	60	>99	~99
G@CALB- Cu(0)NPs	30	>99	~99
G@CALB$Cu_3(PO_4)_2$NPs	60	>99	~99
G@TLL	120	0	0
G@TLL-Cu_2ONPs	40	>99	~99
G@TLL-Cu(0)NPs	20	>99	~99
G@TLL$Cu_3(PO_4)_2$NPs	30	>99	~99
G@CALB-Pd(0)NPs	60	>99	~99
G@TLL-Pd(0)NPs	30	>99	~99
G@TLL@CRL	120	0	0
G@TLL@CRL-Cu_2ONPs	120	>99	~99
G@TLL@CRL-$Cu_3(PO_4)_2$NPs	60	>99	~99
G@TLL@CRL-Pd(0)NPs	120	>99	~99
G@CALB@PdNPs-$Cu_3(PO_4)_2$NPs	60	>99	~99
G@TLL@CRL-Pd(0)NPs-$Cu_3(PO_4)_2$NPs	120	>99	~99

c

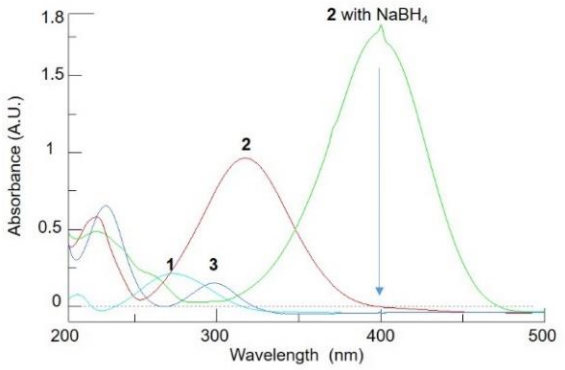

Fig. 6 (a) Scheme of domino cascade; (b) Time-course for full conversion in synthesis of **3** from **1**. Conditions: 12 mM **1**, 20 mg of catalyst, r.t.; (c) UV absorption spectra of the reaction catalyzed by **G@CALB-Pd(0)NPs-$Cu_3(PO_4)_2$NPs**. The adsorption peak at 400 nm (corresponding to the concentration of **2**), time-depending quickly decreased in intensity with a contemporary appearance of an increasing shoulder at 300 nm, indicating the reduction of **2** to **3**.

The multiple three-and four catalytic system were tested (Fig. 6). The coating of the enzyme preparation with a second lipase (CRL) showed hybrids with lower efficiency, being the best **G@TLL@CRL-$Cu_3(PO_4)_2$NPs**, which complete the cascade in 60 min. Gain the differences in efficiency with Pd catalyst was mainly due to the highest enzymatic activity retained in the hybrid. **G@CALB-Pd(0)NPs-$Cu_3(PO_4)_2$NPs** also maintained good enzymatic activity (approx. 50%) completing the cascade process in 60 min. Surprisingly, in the direct transformation of **2** to **3** (the non-limiting reaction in the domino process), the **G@CALB-Pd(0)NPs/$Cu_3(PO_4)_2$NPs** hybrid

exhibited a tremendous efficiency in term of metallic activity, completing the reduction in seconds at different concentrations (Fig. S43), even in 30 seconds at 67 mM concentration (maximum solubility of **1** in water) (Fig. S43). This catalyst showed a TOF value (calculated at 10 mM concentration) of 20570 s^{-1}, *as far as we know*, the faster in this reaction and it was possible to synthesize 500 mg of **3** in 30 seconds using 25 mg of catalyst. The efficiency of the Pd/Cu catalyst was >50 times higher than for **G@CALB-Pd(0)NPs** (TOF value of 397 s^{-1}) and >40000 times higher than for **G@CALB-$Cu_3(PO_4)_2$NPs** (TOF value of 0.5 s^{-1}). This extremely high activity could be explained by a synergistic effect between Pd and Cu considering that this hybrid presents PdCu alloy nanoparticles (Fig. S34). Reported studies in the literature described that mutual interaction between the metals in an alloy of PdCu could modify the electronic properties and resulted to high activity and stability.[54-55] It has also been postulated that the presence of PdO oxide layer is advantageous for the catalytic performance of a PdCu system. Finally in order to evaluate a three-step cascade system, the one-pot cascade was evaluated using **G@CALB-Pd(0)NPs-$Cu_3(PO_4)_2$NPs** in the transformation of **1** to benzoquinone (**4**), combining enzymatic hydrolysis, palladium amino-hydrogenation and copper oxidation (Fig. 7). The cascade to **3** was then complete with a step in the presence of hydrogen peroxide. The hybrid was able to produce **4** in 65 min**.** **G@CALB-Pd(0)NPs** was also tested in this cascade, and no **4** formation was obtained, demonstrating that this step was due to copper nanoparticles.

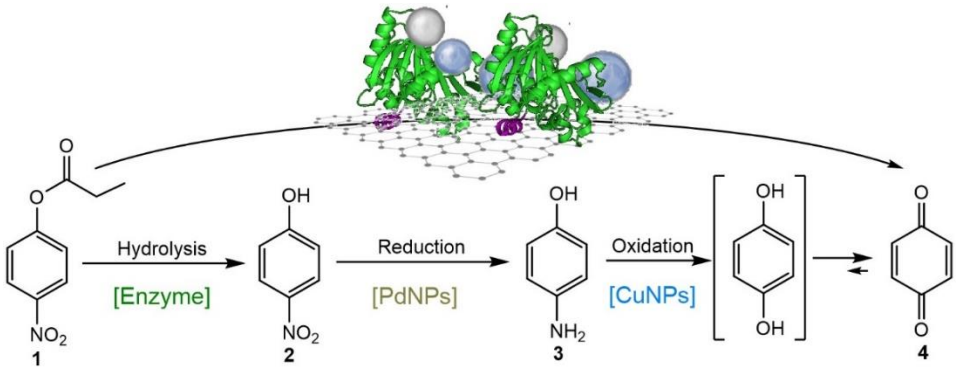

Fig. 7 Domino system combining combo chemocatalysis by **G@CALB-Pd(0)NPs-$Cu_3(PO_4)_2$NPs** in the transformation of p-nitrophenyl propionate (**1**) to benzoquinone (**4**).

Catalytic performance of biohybrids in chemoenzymatic cascade reaction in carbohydrate chemistry

Aiming to further expand the applicability of the complex system, different hybrids were used in two different cascade processes to synthesize high-added value building blocks in carbohydrate chemistry (Fig. 8).[53] First cascade tested involved enzymatic hydrolytic activity followed by metallic oxidative activity of **G@CALB-CuNPs** hybrids to transform peracetylated glucose (**5)** (Fig. 8).

Before to apply the system in cascade, we evaluated the two activities separately. In terms of CALB activity, all hybrids showed excellent regioselectivity to the monodeprotection in C-3 with a yield of **6** of higher than 99% in 20 h in buffer solution at r.t. (Fig. 8a). Then, the Cu efficiency in the oxidation of **6** was tested in aqueous solution and r.t. (Fig. 8b). No conversion was obtained when the reaction was performed with concentration of hydrogen peroxide lower than 125 mM.

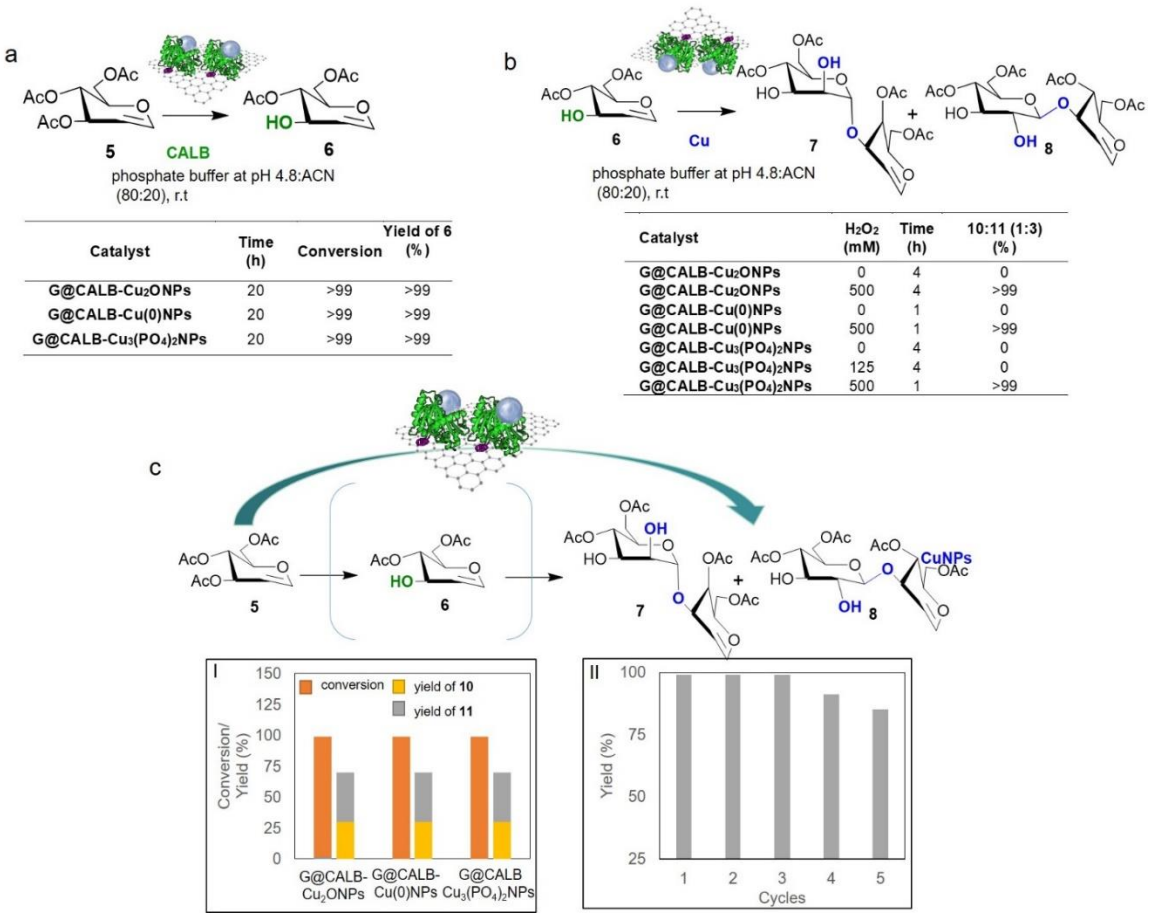

Catalyst	Time (h)	Conversion	Yield of 6 (%)
G@CALB-Cu_2ONPs	20	>99	>99
G@CALB-Cu(0)NPs	20	>99	>99
G@CALB-$Cu_3(PO_4)_2$NPs	20	>99	>99

Catalyst	H_2O_2 (mM)	Time (h)	10:11 (1:3) (%)
G@CALB-Cu_2ONPs	0	4	0
G@CALB-Cu_2ONPs	500	4	>99
G@CALB-Cu(0)NPs	0	1	0
G@CALB-Cu(0)NPs	500	1	>99
G@CALB-$Cu_3(PO_4)_2$NPs	0	4	0
G@CALB-$Cu_3(PO_4)_2$NPs	125	4	0
G@CALB-$Cu_3(PO_4)_2$NPs	500	1	>99

Fig. 8. (a) Regioselective enzymatic hydrolysis of peracetylated glucal **5** catalyzed by **G@CALB-CuNPs** hybrids; (b) Synthesis of disaccharides **7** and **8** from **6** by Cu catalysis from different hybrids in the presence of different amounts of hydrogen peroxide; (c) Direct cascade reaction from **5** to produce regioselectivity **7** and **8** catalyzed by Cu-hybrids. (I) Conversion and yield of the different hybrids after 24 h reaction in the presence of 500 mM of H_2O_2; (II) Reaction yield of five cycles using **G@CALB-$Cu_3(PO_4)_2$NPs** in the conversion of **5** to **7** and **8**.

However, full conversion was obtained in 1 h of reaction time in all cases in the presence of 500 mM H_2O_2 (Fig. 8b) using **G@CALB-Cu(0)NPs** or **G@CALB-$Cu_3(PO_4)_2$NPs**, whereas 4 h of reaction time were necessary when **G@CALB-Cu_2ONPs** was the catalyst. The product obtained in this reaction was isolated and characterized by NMR and mass spectrometry to confirm the formation of new disaccharides **7** and **8** in 3:1 ratio (Fig. S44-S50). A possible explanation to the disaccharide's formation starts with the oxidation by Cu of the double bond in **6** to affords an

epoxide, which then it was directly attacked by free OH of **6** molecules to yield **7** and **8** (Fig. S51).[56-57] Chemoenzymatic cascade process transformation of **5** to **7** and **8** was complete for the hybrids in 24 h (28 h for **G@CALB-Cu_2ONPs**) (Fig. 8c-I). In order to demonstrate the applicability of this system, a recycling experiment was performed using **G@CALB-$Cu_3(PO_4)_2$NPs**. 85% of the initial efficiency was conserved after five cascade cycles (Fig. 8c-II).

In a second cascade process, we evaluate the capacity of CRL to selectively hydrolyze peracetylated glucose (**9**), followed by oxidative capacity of Cu, as well as the potential synergistic effect of the Pd/Cu combination (Fig. 9). As previously, we first evaluated the two steps separately with the different G@TLL@CRL-Pd-Cu hybrids (Fig. 9a). All these hybrids showed enzymatic activity with excellent selectivity towards a monodeprotection at C-6, producing >99% of **10** after 96 h in aqueous solution at r.t. The activity and regioselectivity exclusively of CRL were demonstrated, because no conversion was observed when the **G@TLL-CuNPs** hybrids were used (data not shown). Starting from **10**, the metallic-activity of the different hybrids was tested (Fig. 9b). The Cu-hybrids were catalytically active in the presence of H_2O_2, while the Pd-hybrid was not effective (Fig. 9b). The hybrids showed different efficiency depending on the Cu species and size. **G@TLL@CRL-$Cu_3(PO_4)_2$NPs** was the most efficient, with a full conversion of **10** in **11** after 72 h. The hybrids containing $Cu_3(PO_4)_2$NPs showed the best efficiency (Fig. 9b) with a complete transformation in 72 h, whereas **G@TLL@CRL-Cu_2ONPs** showed 50% conversion after 120h. The product obtained in this reaction was isolated and characterized by NMR as the diacetylated-gluconic acid derivative **11** (Fig. S52-S54).

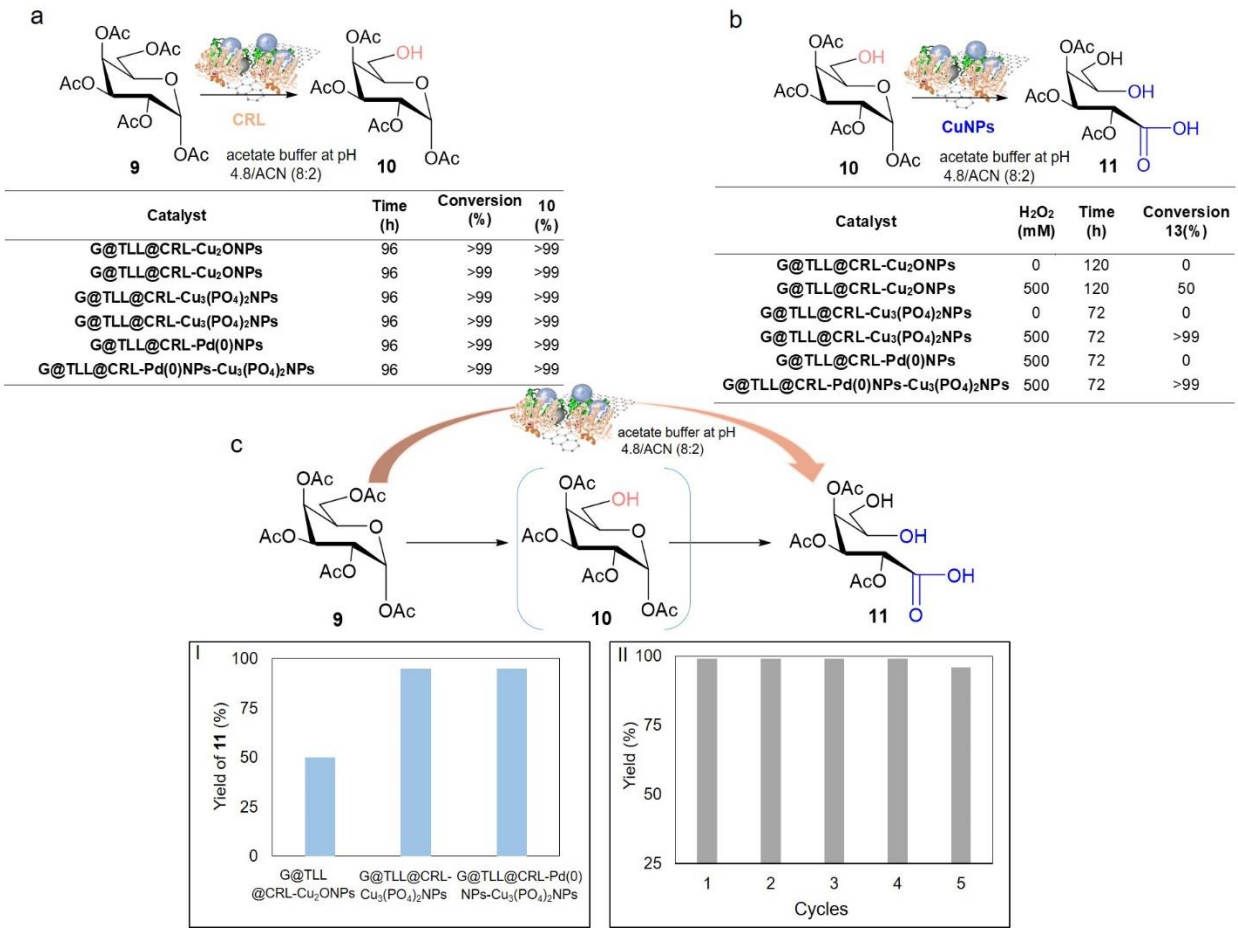

Catalyst	Time (h)	Conversion (%)	10 (%)
G@TLL@CRL-Cu_2ONPs	96	>99	>99
G@TLL@CRL-Cu_2ONPs	96	>99	>99
G@TLL@CRL-$Cu_3(PO_4)_2$NPs	96	>99	>99
G@TLL@CRL-$Cu_3(PO_4)_2$NPs	96	>99	>99
G@TLL@CRL-Pd(0)NPs	96	>99	>99
G@TLL@CRL-Pd(0)NPs-$Cu_3(PO_4)_2$NPs	96	>99	>99

Catalyst	H_2O_2 (mM)	Time (h)	Conversion 13(%)
G@TLL@CRL-Cu_2ONPs	0	120	0
G@TLL@CRL-Cu_2ONPs	500	120	50
G@TLL@CRL-$Cu_3(PO_4)_2$NPs	0	72	0
G@TLL@CRL-$Cu_3(PO_4)_2$NPs	500	72	>99
G@TLL@CRL-Pd(0)NPs	500	72	0
G@TLL@CRL-Pd(0)NPs-$Cu_3(PO_4)_2$NPs	500	72	>99

Fig. 9 (a) Regioselective enzymatic hydrolysis of peracetylated glucose **9** catalyzed by nanobiohybrids. (b) Synthesis of **11** from **10** from different hybrids. (c) Direct cascade reaction from **9** to produce regioselectively **11** catalyzed by Cu-hybrids. (i) Conversion and yield of the different hybrids after 72 h reaction in the presence of 500 mM of H_2O_2. (ii) Reaction yield of five cycles using **G@TLL@CRL-Pd(0)NPs-$Cu_3(PO_4)_2$NPs** in the conversion of **9** to **11.**

After the control experiments, the cascade starting from **9** was attempted (Fig. 9c-I). **G@TLL@CRL-$Cu_3(PO_4)_2$NPs** was able to transform **9** to **11** in >95% yield after 72h, while **G@TLL@CRL-Cu_2ONPs** showed, as previously in the metallic step, low efficiency with only 50% yield after this incubation time (Fig. 9c-I). The oxidation process was clearly caused by the Cu, the hybrid **G@TLL@CRL-Pd(0)NPs** did not produce oxidation of **10** (data not shown).

The bimetallic hybrid **G@TLL@CRL-Pd(0)NPs-$Cu_3(PO_4)_2$NPs** showed full conversion to **11** after 72 h**.** Synergistic effect was clearly demonstrated, and the multienzymatic hybrid showed a better performance in the cascade process in a one-compartment system, improving the catalytic efficiency 200% respect to the reaction in separate steps. The applicability of the complex system **G@TLL@CRL-Pd(0)NPs-$Cu_3(PO_4)_2$NPs** was evaluated in a recycling experiment. After 5 cycles at optimal condition, the catalyst conserved >95% efficiency in the cascade process (Fig. 9c-II).

Catalytic performance of hybrids in Dynamic kinetic resolution

Finally, in order to scope the applicability of these new multiactive heterogeneous catalysts in asymmetric catalysis, the dynamic kinetic resolution of *rac*-phenylethylamine **12** in organic solvent was attempted (Table 1). Lipase CALB has been described to show enantioselective transesterification of **12** toward the *R* enantiomer.[30-31] Therefore, hybrids **G@CALB-Pd(0)NPs** and **G@CALB-Pd(0)NPs-$Cu_3(PO_4)_2$NPs** were used as catalysts in the tandem process.

First, **G@CALB-Pd(0)NPs** was used as catalyst. *Rac*-**12** was transformed in *R*-**14** at almost quantitative conversion and excellent enantiopurity (ee>99%) in 36h using ethyl acetate as acylating agent in toluene at 70ºC (Table 1). The reaction was also tested in THF although the conversion was quite low and Pd was leached from the catalyst. Next **G@CALB-Pd(0)NPs-$Cu_3(PO_4)_2$NPs** was used as catalyst (containing 0.03% mol CALB, 20% mol Pd and 200% mol Cu), in the DKR, showing a best performance, with a complete conversion of enantiopure *R*-**14** in 20 h in toluene, demonstrating also in this process the synergistic effect of Pd and Cu[58] in racemization. This catalyst was also used 3 times, and activity and selectivity were conserved.

Table 1. Dynamic Kinetic resolution catalyzed by biohybrids.[a]

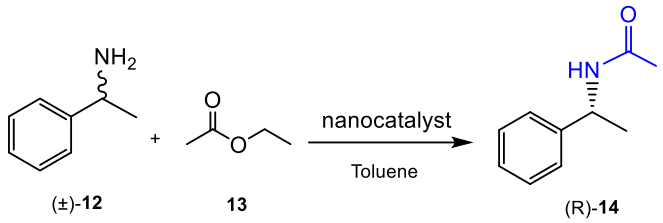

Catalyst	Solvent	Time (h)	*C* (%)[c]	ee (%)[d]
G@CALB-Pd(0)NPs[a]	Toluene	36	>99	>99
G@CALB-Pd(0)NPs[a]	THF[b]	67	40	nd
G@CALB-Pd(0)NPs-$Cu_3(PO_4)_2$NPs[a]	Toluene	20	>99	>99

[a]Reaction conditions: **12** (0.01 mmol), **13** (0.06 mmol), toluene (1 mL), 200 mg catalyst, 70ºC.[b] Pd was leached from the catalysts. [c]Conversion calculated by RP-HPLC analysis.[d] ee: enantiomeric excess determined by chiral HPLC. nd: not determined.

Conclusion

Enzyme-graphene nanometal hybrids as multiactive heterogeneous catalysts have been designed and synthesized. The *in-situ* formation of metallic nanoparticles of different size and species on multilayer graphene-anchored enzymes allowed to create different kind of enzyme-metal nanoarchitectures, containing up to two different enzymes and two different metal nanoparticles in the same compartment. The cooperative and synergistic participation from different chemo- and biocatalytic components of them was demonstrated in the reduction process and especially in different cascade reactions. Domino cascade in aqueous media (enzymatic hydrolysis, metal reduction, and metal oxidation) was successfully performed from the different hybrid systems. Also, the successful application of enzyme-metallic systems in the dynamic kinetic resolution of racemic arylamine in organic solvent demonstrated the potential effect in synthetic chemistry, and the synergistic effect of CALB, Pd and Cu catalysis. Finally, the different systems were applied in

the synthesis of interesting glycoderivatives, by chemoenzymatic cascade processes, transforming peracetylated glucal to selectively novel disaccharides molecules for example using **G@CALB-$Cu_3(PO_4)_2$NP**s and **G@CALB)-Cu(0)NPs** as the best catalysts. The cascade reaction starting from α-peracetylated glucose to synthesize a diacetyl-gluconic acid, interesting building block in carbohydrate chemistry, was efficiency performed by **G@TLL@CRL-Pd(0)NPs-$Cu_3(PO_4)_2$NPs** Furthermore, recycling studies demonstrated the high robustness of these systems, maintaining more than 95% activity after 5 cycles of used. These excellent results in one-pot cascade processes open the potential application as catalytic platform for other complex pharmaceutical synthesis and in the field of biomedicine and biotechnology.

Experimental section

General synthesis of G@Enzyme-CuNPs hybrids

500 mg of G@TLL (containing 3 mg of *Thermomyces lanuginosus* lipase (TLL)) or G@CALB (3.5 mg of *Candida antarctica* B lipase (CALB)) were added to 8 ml buffer 0.1M (sodium bicarbonate pH = 10 or sodium phosphate pH 7) in a 75 ml glass vial containing a small magnetic bar stirrer. Then, 80 mg of $Cu_2SO_4 \cdot 5H_2O$ (10 mg/mL) were added to the solution with the support and it was maintained for 16 hours. After 16 h, 800 µL of $NaBH_4$ (45 mg) aqueous solution (1.2 M) was added to the black solution obtaining a final concentration of 0.12 M sodium borohydride in the mixture. The mixture was reduced for 30 min. After incubation, the mixture was centrifuged at 8000 rpm for 20 min. The sediment generated was re-suspended in 5 ml of water. It was centrifuged again at 8000 rpm for 20 min and the supernatant was removed. The process was repeated two more times. Finally, the supernatant was removed and the pellet was re-suspended in 2 mL of water and added to a cryogenization tube, frozen with liquid nitrogen and lyophilized

overnight. After that, the so-called **G@TLL-Cu(0)NPs** and **G@CALB-Cu(0)NPs** for pH 10 conditions and **G@TLL-Cu_2ONPs** and **G@CALB-Cu_2ONPs** for pH 7 conditions were obtained.

Another variation of the phosphate protocol was used, in which the reduction step was not performed. **G@TLL-$Cu_3(PO_4)_2$ NPs** and **G@CALB-$Cu_3(PO_4)_2$NPs**, were obtained respectively.

General synthesis of G@Enzyme-Pd(0)NPs hybrids

500 mg of G@TLL (containing 3 mg of *Thermomyces lanuginosus* lipase (TLL)) or G@CALB (3.5 mg of *Candida antarctica* B lipase (CALB)) were added to 20 ml distilled water in a 75 ml glass vial containing a small magnetic bar stirrer. Then, 25 mg of $Pd(OAc)_2$ was dissolved in 5 mL of MeOH and this Pd solution was added to the solution with the support and the mixture was maintained for 24 hours. After that, the mixture was centrifuged at 8000 rpm for 20 min. The sediment generated was re-suspended in 5 ml of MeOH:water (1:5), two times and a third centrifugation with only distilled water was made. Finally, the supernatant was removed and the pellet was re-suspended in 2 mL of water and added to a cryogenization tube, frozen with liquid nitrogen and lyophilized overnight. After that, the so-called **G@CALB-Pd(0)NPs** and **G@TLL-Pd(0)NPs** were obtained.

General synthesis of G@TLL@CRL-CuNPs hybrids

500 mg of G@TLL@CRL were added to 20 mL buffer sodium phosphate 0.1M pH 7 in a 50 ml glass vial containing a small magnetic bar stirrer. Then, 200 mg of $Cu_2SO_4 \cdot 5H_2O$ (10 mg/mL) were added to the solution with the support and it was maintained for 16 hours. After 16 h, 2 mL of $NaBH_4$ (112 mg) aqueous solution (1.2 M) was added to the black solution obtaining a final concentration of 0.12 M sodium borohydride in the mixture. The mixture was reduced for 30 min. After incubation, the mixture was centrifuged at 8000 rpm for 20 min. The sediment generated

was resuspended in 5 ml of water. It was centrifuged again at 8000 rpm for 20 min and the supernatant was removed. The process was repeated two more times. Finally, the supernatant was removed and the pellet was resuspended in 2 mL of water and added to a cryogenization tube, frozen with liquid nitrogen and lyophilized overnight. After that, the so-called **G@TLL@CRL-Cu_2ONPs** was obtained. Another variation of the protocol was used, in which the reduction step was not performed, and the so-called **G@TLL@CRL-$Cu_3(PO_4)_2$NPs** was obtained.

General synthesis of G@TLL@CRL-Pd(0)NPs hybrid

500 mg of G@TLL@CRL were added to 50 ml distilled water in a 100 ml glass vial containing a small magnetic bar stirrer. Then, 62 mg of $Pd(OAc)_2$ was dissolved in 7 mL of MeOH and the solution was added to the solution with the support and it was maintained for 24 hours. After incubation, the mixture was centrifuged at 8000 rpm for 20 min. The sediment generated was resuspended in 10 ml of MeOH:water (1:5) two-fold and a third centrifugation with only distilled water. Finally, the supernatant was removed and the pellet was resuspended in 2 mL of water and added to a cryogenization tube, frozen with liquid nitrogen and lyophilized overnight. After that, the so-called **G@TLL@CRL-Pd(0)NPs** was obtained.

Synthesis of G@Enzyme-Pd(0)NPs-$Cu_3(PO_4)_2$ NPs hybrids

500 mg of **G@TLL@CRL** or **G@CALB** were added to 50 ml or 20 ml distilled water, respectively, in a glass vial containing a small magnetic bar stirrer. Then, 62 or 25 mg of $Pd(OAc)_2$ were dissolved in 12 or 5 mL of MeOH, respectively. The Pd solution was added to the graphene solution and the reaction was maintained by magnetic stirring for 24 h. After incubation, the mixture was centrifuged at 8000 rpm for 20 min. The sediment generated was resuspended in 10

ml of MeOH:water (1:5) two-fold and a third centrifugation with only distilled water. Finally, the supernatant was removed and the pellet were added to 20 mL or 8 ml, respectively, of buffer sodium phosphate 0.1M pH 7 in a 25 ml glass vial containing a small magnetic bar stirrer. Then, 200 or 80 mg of $Cu_2SO_4 \cdot 5H_2O$ (10 mg/mL) were added, respectively, to the solution with the support and the mixture was maintained for 16 hours. After incubation, the mixture was centrifuged at 8000 rpm for 20 min. The sediment generated was resuspended in 5 ml of water. It was centrifuged again at 8000 rpm for 20 min and the supernatant was removed. The process was repeated two more times. Finally, the supernatant was removed and the pellet was resuspended in 2 mL of water and added to a cryogenization tube, frozen with liquid nitrogen and lyophilized overnight. After that, the so-called **G@TLL@CRL-Pd(0)NPs-$Cu_3(PO_4)_2$NPs, G@CALB-Pd(0)NPs-$Cu_3(PO_4)_2$NPs** were obtained.

Enzymatic pNPP activity assay: hydrolysis of 4-nitrophenyl propionate (1)

This assay was performed by measuring the increase in the absorbance at 348 nm produced by the release of p-nitrophenol in the hydrolysis of 0.4 mM (**1**) in 25 mM sodium phosphate buffer at pH 7 and 25 ºC. To initialize the reaction, 3mg of solid was added to 5 mL of substrate solution, measuring the absorbance at different times. In the case of lipase solution, 20 µL was added to 2.5 mL of substrate solution. The enzymatic activity was expressed in specific activity per amount of protein (U/mg). The specific activity (U/mg) was calculated using the following equation:

$$U(\mu mol \cdot min^{-1} \cdot mg^{-1}) = \frac{\Delta Abs/\min \cdot V}{\varepsilon \cdot mg_{protein}}$$

where the molar extinction coefficient (ε) used was 5.15 mL/µmol·cm, and mg of enzyme.

Metallic activity of hybrids: catalytic reduction of 4-nitrophenol (2) to 4-aminophenol (3)

p-Nitrophenol (**2**) was dissolved in 2 mL of distilled water at to 1-10 mM concentration. Then, $NaBH_4$ (40mM) was added to the solution. After this addition, the light-yellow solution changes to a strong yellow colour, generating the formation of 4-nitrophenolate ions (substrate UV-peak undergoes to an immediate shift from 317 to 400 nm). After 30 seconds, catalysts were added under gentle stirring at room temperature in an orbital shaker. These catalysts were selected because they have the Cu (0) and Pd (0) species, respectively. The reaction progress was monitored by taking out an aliquot of the solution (0.1 mL) at different times, diluting it with distilled water (2 mL) and measuring the absorption spectrum between 500 and 300 nm in a quartz cuvette.

Domino Synthesis of 4-aminophenol (3) from 4-nitrophenyl propionate (1)

97.6 mg of **1** were dissolved in 10mL of ACN. 60 µL of the previous solution were added to 2.4 mL of sodium phosphate buffer pH 7 solution and the mixture was under magnetic stirring at 25 °C until homogenization. Next, 20 mg of solid biohybrid was added. The reaction was kept on gentle stirring until complete conversion of **1** to the product **2** (between 25-120min depending on catalyst). Then, to initialize the reduction of **2** to **3**, the solid $NaBH_4$ (0.001 mol; 0.03 g) was added straight to the reaction mixture under gentle magnetic stirring at 25 °C. The reaction progress was checked by taking out an aliquot of the solution (20 µL), diluting it with water (2 mL), and measuring the absorption spectrum between 600 and 200 nm in a quartz cuvette.

Domino Synthesis of benzoquinone (4) from 4-nitrophenyl propionate (1)

Following the process described arrived using **G@CALB-Pd(0)NPs-$Cu_3(PO_4)_2$NPs** as catalyst, once **3** was obtained, 100 mM of hydrogen peroxide (1%, v/v) were added and gently shaken at

room temperature in an orbital shaker (320 rpm). Samples (100 µL) were taken at different times and the reaction was followed by HPLC. Samples were first centrifuged at 8,000 rpm for 5 min and then diluted 50 µL 20-fold in bidistilled water before injection. The HPLC column was C8 Kromasil 150 x 4.6 mm AV-2059. HPLC conditions were: an isocratic mixture of 15% acetonitrile and 85% bi-distilled water, UV detection at 270 nm, and a flow rate of 0.4 mL/min. Under these conditions, the retention times of **4**, **3** and H_2O_2 were 15.3 min, 9 min and 4 min, respectively.

Cascade reaction synthesis of disaccharides 7/8 from peracetylated glucal (5) catalysed by G@CALB-CuNPs hybrids

Tri-*O*-acetyl-D-glucal (25 mg) (**5**) was dissolved in 5 mL of 50 mM sodium phosphate buffer at pH 4.8, containing in 20% of ACN. Then, 500µL of H_2O_2 and 750 mg of catalyst were added. The reaction was followed by TLC and HPLC analysis at different times at room temperature. For the TLC measurement, hexane: ethyl acetate (1:1) was used as eluent. The products were detected by spraying the TLC plate completely with a 10% (v/v) solution of H_2SO_4 in methanol and on a hot plate where light brown spots appeared on the surface of the plate. The HPLC conditions were an isocratic mixture of 70:30 water:ACN as mobile phase, UV detection at 215 nm, and a flow rate of 1 mL/min. Under these conditions, retention times of Tri-*O*-acetyl-D-glucal (**5**), α-3-OH diacetylated (**6**) and **7/8** were 11.5, 3.5 and 2.2/2.8 min, respectively. As an additional experiment it was tested without and with 25 µL of H_2O_2. For product characterization, after reaction complete the product was separated from the catalyst (**G@CALB-$Cu_3(PO_4)_2$NPs)** by centrifugation and the supernatant (aqueous phase) was transferred to a 250 ml separator funnel and the aqueous phase was extracted with ethyl acetate (9 x 20 ml). Subsequently, the collected organic phases were dried by adding about 1.5 g of anhydrous sodium sulphate. After 5 min, the mixture was filtered by gravity through a fluted filter paper in a funnel to remove sodium sulphate, and collect the liquid

in a 250 ml round bottom flask. Solvent was removed using a BUCHI rotary evaporator at 40° C under vacuum aspirator (200 mbar), obtaining a white powder (18 mg) Products were full characterized and identified by NMR and ESI-MS (Fig. S44-S50).

Cascade reaction synthesis of 11 from peracetylated glucose (9) catalysed by G@TLL@CRL-CuNPs hybrids

α-*D*-glucose pentaacetate (25 mg) (**9**) was dissolved in 10 mL of 50 mM sodium acetate buffer at pH 4.8, containing in 20% of ACN (v/v). Then, 500µL of H_2O_2 and 750 mg of catalyst were added. The reaction was followed by TLC and HPLC analysis at different times and room temperature. For the TLC measurement, hexane: ethyl acetate (1:1) was used as eluent. The products were detected by spraying the plate completely with a 10% (v/v) solution of H_2SO_4 in methanol and on a hot plate where light brown spots will appear on the surface of the plate. The HPLC conditions were an isocratic mixture of 70:30 water:ACN as mobile phase, UV detection at 215 nm, and a flow rate of 1 mL/min. Under these conditions, retention times of α-*D*-glucose pentaacetate (**9**), α-6-OH (**10**) and product **11** were 16.5, 5.5 and 2.5 min, respectively.

For product isolation, after reaction complete, the product was separated from the catalyst (**G@TLL@CRL-$Cu_3(PO_4)_2$NPs)** by centrifugation and the supernatant (aqueous phase) was transferred to a 250 ml separatory funnel and the aqueous layer was extracted with ethyl acetate (9 x 20 ml). Subsequently, the organic layer was dried by adding about 1.5 g of anhydrous sodium sulfate. Shake gently for 5 min, filter the mixture by gravity through a fluted filter paper in a funnel to remove sodium sulfate, and collect the filtrate in a 250 ml round bottom flask. Evaporate the solvent using a rotary evaporator at 40° C under vacuum aspirator (200 mbar) to obtain the product.^{1}H NMR (400.13 MHz, D_2O, 25 °C): δ= 6.17 (d, J = 3.6 Hz, 1H, H-2), 5.27 (t, J = 10 Hz, 1H, H-4), 5.03 (dd, J = 10 Hz, J = 4 Hz, 1H, H-3), 4.28, 4.04 (AB part of an ABX spin system,

2H, CH_2-H6a,b), 3.78 (dd, J = 10 Hz, J = 9.2 Hz, 1H, H-5), 2.15 (s, 3H, Ac), 2.06 (s, 3H, Ac), 2.04 (s, 3H, Ac).^{13}C NMR (100.61 MHz, D_2O, 25 °C): δ= 174.23 (2C collapsed, C=O), 172.18 (C=O), 89.16 (C-2), 71.73 (C-6), 20.30 (Me), 20.18 (2C collapsed, Me). No more ^{13}C could be determined. ^{13}C chemical shifts were obtained from edited-HSQC and HMBC 2D ^{1}H-^{13}C correlation spectra. Despite large accumulation trials, no signals were found in the ^{13}C APT spectrum.

Dynamic kinetic resolution (DKR) of (±)-1-phenylethylamine (**12**)

The acylating agent (ethyl acetate **13**, 6 µl, 0.06 mmol) was added to a screw-sealed vessel containing **12** (1.3 µL, 0.01 mmol,) in toluene (1 mL). The mixture was kept at 70 °C under vigorous magnetic stirring for 5 min. After that, to initialize the reaction, 200 mg of catalyst were added. The final suspension was left under vigorous magnetic stirring at 70 °C for the indicated times. The reactions were monitored by TLC, RP-HPLC analysis of the reaction's samples withdrawn at different times. The analysis conditions were as a mobile phase hexane:ethyl acetate 45:55 (v/v) at 25 °C. The analysis conditions were column: Kromasil Ultrabase C18 (250 x 4.6 mm, 5 µmø), flow of 1 mL/min; λ: 254 nm; mobile phase: 30% (v/v) ACN in MilliQ water 0.1% (v/v) trifluoroacetic acid and temperature: 25 °C. R_t of **12** was 3.24 min whereas R_t of acetylated product **14** was 7.0 min. The standard reference compounds ((R/S), R or S-**14**) were prepared by treating **12** with few drops of acetic anhydride into the vial. The different samples were diluted (1:1) with the mobile phase and centrifuged before injection. Each sample was injected in triplicate.

The enantiomeric excess (ee) value was determined by chiral HPLC analysis of the reaction's samples withdrawn at final time. The analysis conditions were: Phenomenex Lux Cellulose-1 (250 x 4.6 mm, 3 µmø) column, flow of 0.3 mL / min; λ: 210 nm; mobile phase: 90:10 (v/v) n-Hexane-

isopropanol. R_t of S-**14** was 24 min whereas R_t of R-**14** was 26 min. The different samples were diluted (1:1) with the mobile phase and centrifuged before injection. Each sample was injected in triplicate.

Data availability

The data supporting the findings of this study are available within the article and in the ESI.

Author contributions

JMP: conceptualization, methodology, project administration, writing – reviewing and editing, supervision, funding acquisition. NL-G: investigation, validation, writing – original draft. EU: methodology, writing – reviewing & editing, funding acquisition. All authors discussed the results and were involved in manuscript writing.

Conflicts of interest

There are no conflicts to declare.

Acknowledgments

This work was supported by the Spanish Government and the Spanish National Research Council (CSIC) (projects PIE 201980E081 and MCIN/AEI/10.13039/501100011033, Project No. PID2019-106394GB-I00/AEI/10.13039/501100011033), and also by the Gobierno de Aragón-

FSE (Spain, research group Aminoácidos y Péptidos E19_20R). The authors thank Dr. Martinez from Novozymes for the gift of CALB and TLL enzymes.

Notes and references

1. G. Ciulla, S. Zimmermanna, K. Kumar. *Org. Biomol. Chem*., 2019,**17**, 413-431

2. N. Losada-Garcia, Z. Cabrera, P. Urrutia, C. Garcia-Sanz, A. Andreu, J.M. Palomo. *Catalysts*, 2020, **10**, 1258.

3. M. B. Li, J.E. Bäckvall. *Acc. Chem. Res*. 2021, **54**(9), 2275-2286.

4. D. Kracher, R. Kourist. *Curr. Opin. Green Sustain. Chem*. 2021, **32,** art. no. 100538

5. Y. Ge, F. Ye, J. Yang, A. Spannenberg, H. Jiao, R. Jackstell, M. Beller. *Angew. Chem. Int. Ed.* 2021, **60** (41), 22393-22400

6. Q. Chen, G.-S. Luo, Y.-J. Wang. *Green Chem*. 2021, **23** (18), 7074-7083.

7. M. Sohail, F. Tanaka. *Angew. Chem. Int. Ed.* 2021, **60**(39), 21256-21260

8. X.-Y. Chai, H.-B. Xu, L. Dong. *Chem. Eur. J.* 2021, **27** (52), 13123-13127.

9. J.M. Woodley. *Curr. Opin. Green Sustain. Chem.* 2020, **21**, 22–26.

10.R.A. Sheldon, J.M. Woodley. *Chem. Rev*. 2018, **118**, 801–838.

11. F. Rudroff, M. D. Mihovilovic, H. Gröger, R. Snajdrova, H. Iding, U. T. Bornscheuer. *Nat. Catal*. 2018, **1**, 12–22.

12. A.D. Liang, J. Serrano-Plana, R.L. Peterson, T.R. Ward. *Acc. Chem. Res*. 2019, **52** (3), 585-595.

13. C. Garcia-Sanz, A. Andreu, B. de las Rivas, A.I. Jiménez, A. Pop, C. Silvestru, E.P. Urriolabeitia, J.M. Palomo. *Org. Biomol. Chem*. 2021, **19**, 2773-2783.

14. W. Xu, Z. Fu, G. Chen, Z. Wang, Y. Jian, Y. Zhang, G. Jiang, D. Lu, J. Wu, Z. Liu, *Nat. Commun*. 2019, **10**, 2684.

15. M. Filice, O. Romero, J. Gutierrez-Fernandez, B. de las Rivas, J.A. Hermoso, J.M. Palomo. *Chem. Commun*. 2015, **51**, 9324-9327.

16. M. Filice, O. Romero, A. Aires, J.M. Guisan, A. Rumbero, J.M. Palomo. *Adv. Synth. Catal*. 2015, **357**, 2687-2696.

17. K. P. Gustafson, T. Görbe, G. de Gonzalo-Calvo, N. Yuan, C. L. Schreiber, A. Shchukarev, C-W. Tai, I. Persson, X. Zou, J. E. Bäckvall. *Chem. Eur. J.* 2019, **25**, 9174-9179.

18. R. Chapman, M. H. Stenzel. *J. Am. Chem. Soc*. 2019, **141**, 2754– 2769.

19. D. Hebbalalu, J. Lalley, M. N. Nadagouda, R. S. Varma. *ACS Sustain. Chem. Eng*., 2013, **1**, 703-712.

20. M. Filice, J. M. Palomo. *ACS Catal*. 2014, **4**, 5, 1588-1598.

21. R. Ghosh-Chaudhuri, S. Paria. *Chem. Rev.* 2012, **112**(4), 2373-2433.

22. Z. Cai, J. Dai, W. Li, K. B. Tan, Z. Huang, G. Zhan, J. Huang, Q. Li. *ACS Catal*. 2020, **10**(22), 13275-13289.

23. Z. Li, J. Liu, Z. Huang, Y. Yang, C. Xia, F. Li. *ACS Catal*. 2013, **3**(5), 839-845.

24. J. Ge, J. D. Lei, R. Zare. N. *Nat. Nanotechnol*, 2012, **7**, 428-432.

25. C. Arib, J. Spadavecchia, M. L. de la Chapelle. *Sci. Rep*. 2021, **11**(1), 1-8.

26. N. Parveen, G. Sekar. *J. Org. Chem*. 2020, **85**, 10514–10524.

27. R. Saha, D. Arunprasath, G. Sekar. *J. Org. Chem*. 2018, **83**(8), 4692-4702.

28. J. Izquierdo, M. A. Pericàs. *ACS Catal*. 2016, **6**(1), 348-356.

29. H. A. Döndaş, M. de Gracia Retamosa, J. M. Sansano. *Organometallics*, **2019**, *38*(9), 1828-1867.

30. S. Gao, Z. Wang, L. Ma, Y. Liu, J. Gao, Y. Jiang. *ACS Catal*. 2019, **10**(2), 1375-1380.

31. S. Gao, Y. Liu, L. Wang, Z. Wang, P. Liu, J. Gao, Y. Jiang. *ACS Catal.* 2021, **11**(9), 5544-5553.

32. Y. Liu, P. Liu, S. Gao, Z. Wang, P. Luan, J. González-Sabín, Y. Jiang. *Chem. Eng. J*. 2021, **420**, 127659.

33. H. Zhao, G. Liu, Y. Liu, X. Liu, H. Wang, H. Chen, J. Gao, Y. Jiang. *ACS Appl. Mater. Interfaces.* 2020, **14**, 2, 2881-2892.

34. J.M. Palomo. *Chem. Commun*. 2019, **55**, 9583-9589.

35. R. Benavente, D. Lopez-Tejedor, J.M. Palomo. *Chem. Commun.* 2018, **54**, 6256-6259.

36. M. Filice, M. Marciello, M.P. Morales, J. M. Palomo. *Chem. Commun*. 2013, **49**, 6876-6878.

37. R. Benavente, D. Lopez-Tejedor, M.P. Morales, C. Perez-Rizquez, J.M. Palomo. *Nanoscale*, 2020, **12**, 12917-12927.

38. N. Losada-Garcia, A. Rodriguez-Otero, J.M. Palomo. *Catal. Sci. Technol*., 2020, **10**, 196-206

39. M. Filice, N. Losada-Garcia, C. Perez-Rizquez, M. Marciello, M.P. Morales, J.M. Palomo. *Appl. Nano*, 2021, **2**,1-13.

40. G. Fernández-Lorente, Z. Cabrera, C. Godoy, R. Fernandez-Lafuente, J. M. Palomo, J.M. Guisan. *Process Biochem*. 2008, **43**, 1061–1067.

41. H. Seelajaroen, A. Bakandritsos, M. Otyepka, R. Zboril, N. S. Sariciftci. *ACS Appl. Mater. Inter*. 2020, **12**(1), 250–259.

42. J. J. Zhang, F. Zhang, H. Yang, X. Huang, H. Liu, J.J. Zhang, S. Guo. *Langmuir* 2010, **26** (9), 6083–6085.

43. V. Urbanová, K. Holá, A. B. Bourlinos, K. Čépe, A. Ambrosi, A. H. Loo, M. Pumera, F. Karlický, M. Otyepka, R. Zbořil. *Adv. Mater*. 2015, **27** (14), 2305–2310.

44. K. P. Prasad, Y. Chen, P. Chen. *ACS Appl. Mater. Inter.* 2014, **6** (5), 3387–3393

45. T. Xue, S. Jiang, Y. Qu, Q. Su, R. Cheng, S. Dubin, C. Y. Chiu, R. Kaner, Y. Huang, X. Duan. *Angew. Chem*. 2012, **124**(16), 3888-3891.

46. K.S. Novoselov, V.I. FalKo, L. Colombo, P.R. Gellert, M.G. Schwab, K.A. Kim. *Nature* 2012, **490**, 192–200.

47. F. Bonaccorso, L. Colombo, G. Yu, M. Stoller, V. Tozzini, A.C. Ferrari, R.S. Ruo, V. Pellegrini. *Science* 2015, **347**, 1246501

48. S. Manzeli, D. Ovchinnikov, D. Pasquier, O.V. Yazyev, A. Kis. *Nat. Rev. Mater.* 2017, **2**, 17033.

49. N. Losada-Garcia, A. Berenguer-Murcia, D. Cazorla-Amoros, J. M. Palomo. *Nanomaterials*, 2019, **9**(9), 1344.

50. J. M. Palomo, M. Fuentes, G. Fernández-Lorente, C. Mateo, J.M. Guisan, R. Fernández-Lafuente. *Biomacromolecules*. 2003, **4**,1-6

51. J. Uppenberg, M. T. Hansen, S. Patkar, T. A. Jones. *Structure* 1994, **2**, 293-308; (c) D. M. Lawson, A. M. Brzozowski, S. Rety, C. Verma, G. G. Dodson. *PEDS*. 1994, **7**, 543-550.

52. I. Vlassiouk, M. Regmi, P. Fulvio, S. Dai, P. Datskos, G. Eres, S. Smirnov. *ACS Nano*, 2011, **5**(7), 6069-6076.

53. M. Filice, J. M. Guisan, M. Terreni, J. M. Palomo. *Nat. Protoc.* 2012, **7**, 1783-1796.

54. Y. Liu, W. Li, G. Zhao, G. Qin, Y. Lib, Y. Liu. *Nanoscale* 2021, **13**, 3528-3542.

55. A. Khan, L. Khan, S-I. Khan, A. Badshah. *Electrochim. Act*. 2020, **349**, 136381

56. E. C. Boyd, R. V. H. Jones, P. Quayle, A. J. Waring. *Green Chem.* 2003, **5**, 679–681.

57. M. Kumar, T. R. Reddy, A. Gurawa, S. Kashyap. *Org. Biomol. Chem*. 2020, **18**, 4848–4862.

58. H. Huang, Y. Jin, M. E. Shirbhate, D. Kang, M. Choi, Q. Chen, Y. Kim, S-J. Kim, I-S. Byun, M. Wang, J. Bouffard, S. K. Kim, K. M. Kim. *Nat. Commun*. 2021, **12**(1), 1-7.

Table of Contents

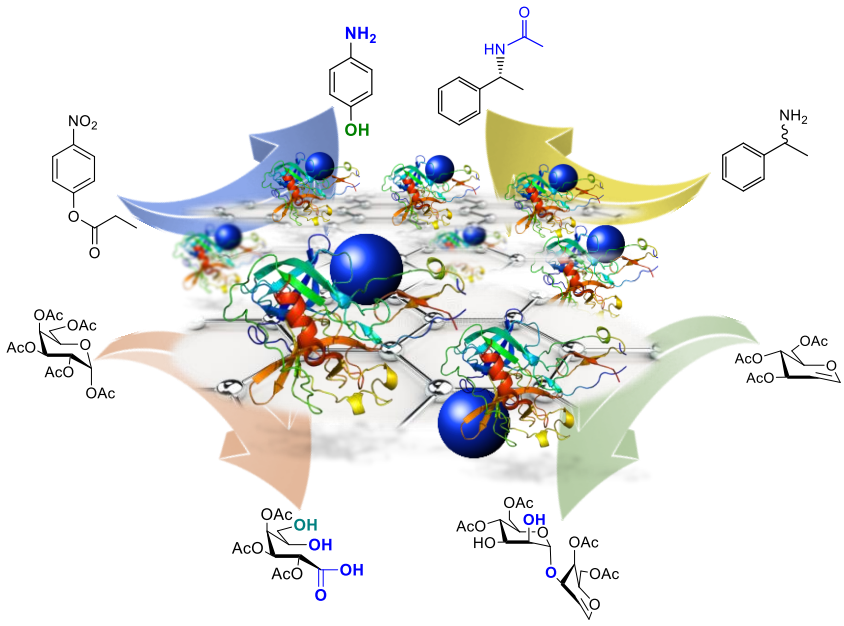

Novel one-compartment enzyme-metal hybrids system as multiactive heterogeneous catalysts with different chemo- and biocatalytic functionalities for sustainable one-pot cascade reactions is described.